Tandem Mass Spectrometry using Continuous-wave Infra-red Multi-photon Dissociation in an Electrostatic Linear Ion Trap

Ian J. Carrick, Kimberly C. Fabijanczuk, Jiayue Rong, Scott A. McLuckey*

Department of Chemistry
Purdue University
560 Oval Drive
West Lafayette, Indiana 47907, United States

Running title: Tandem MS in an ELIT

*Address correspondence to:
Dr. Scott A. McLuckey
560 Oval Drive
Department of Chemistry
Purdue University
West Lafayette, IN 47907-2084, USA
Phone: (765) 494-5270
Fax: (765) 494-0239
E-mail: mcluckey@purdue.edu

ABSTRACT

RATIONALE

The electrostatic linear ion trap (ELIT) can be operated as a multi-reflection time-of-flight (MR-TOF) or Fourier transform (FT) mass analyzer. It has been shown to be capable of performing high resolution mass analysis and high-resolution ion isolations. While it has been used in charge-detection mass spectrometry (CDMS), it has not been widely used as a conventional mass spectrometer (MS) for ensemble measurements of ions, or for tandem-MS. The advantages of tandem-MS with high-resolution ion isolations in the ELIT have thus not been fully exploited.

METHODS

A home-built ELIT was modified with BaF_2 viewports to facilitate transmission of a laser beam at the turnaround point of the second ion mirror in the ELIT. Fragmentation that occurs at the turnaround point of these ion mirrors should result in minimal energy-partitioning due to the low kinetic energy of ions at these points. The laser was allowed to irradiate ions for a period of many oscillations in the ELIT.

RESULTS

Due to the low energy absorption of gas-phase ions during each oscillation in the ELIT, fragmentation was found to occur over a range of oscillations in the ELIT generating a homogeneous ion beam. A mirror-switching pulse is shown to create time-varying perturbations in this beam which oscillate at the fragment ion characteristic frequencies and generate a time-domain signal. This was found to recover FT signal for protonated pYGGFL and pSGGFL precursor ions.

CONCLUSIONS

Fragmentation at the turnaround point of an ELIT by continuous-wave infrared multi-photon dissociation (cw-IRMPD) is demonstrated. In cases where laser power absorption is low and fragmentation occurs over many laps, a mirror-switching pulse may be used to recover varying time-domain signal. The combination of laser activation at the turnaround points and mirror-switching isolation allows for tandem-MS in the ELIT.

Keywords: Infra-red multi-photon dissociation, electrostatic linear ion trap, tandem mass spectrometry

1. Introduction

The electrostatic linear ion trap (ELIT) was introduced in 1997 by Zajfman et al.[1] The ELIT (also referred to as an electrostatic beam ion trap or EBIT) consists of an array of plate electrodes typically positioned around a central pickup electrode used for detection of image charge. Ions can be trapped axially by applying a voltage on each end plate greater than the energy to charge ratio of injected ions. Entrance into the device is accomplished by lowering the entrance plate voltage briefly, although in-trap potential lifts can also be used to lower the energy of injected ions below the trapping threshold.[2] The interior plates provide radial focusing through Einzel lensing, allowing pressure-limited transients in Fourier transform (FT) mode, or separation of ions in a multi-reflectron time-of-flight (MR-TOF) mode.[3,4] In the FT operational mode, the transient is converted to the frequency domain by fast Fourier transformation (FFT), after which the frequency scale is converted to *m/z*. Like other FT instruments, the ELIT performs high-resolution mass analysis, with resolutions above 100,000 FWHM reported.[5,6]

The ELIT design allows for flexibility in the shape of the pickup electrode, as a central field-free region with no ion focusing can be accommodated. This makes it well-suited for charge detection mass spectrometry (CDMS), in which pickup electrodes with high length to diameter ratios are desired for complete image charge formation from single ions.[7] The oscillation of single ions in the device offers the advantage of averaging for minimizing error in charge determination. This feature makes the ELIT geometry well-suited for high performance CDMS. While the ELIT has been shown in early publications to be useful for conventional mass analysis (injection of multiple ions and ion packets),[1,2,4] the ELIT has not been widely adopted for these applications.

While the mass resolution of the ELIT has not been demonstrated to reach that of the commercially available Orbitrap™,[8] ELITs as mass analyzers can be readily fabricated at low cost without sophisticated machining, while achieving mass resolution in the tens of thousands in either FT or MR-TOF modes. Furthermore, the simplicity of the geometry allows for flexibility in constructing variations of the analyzer (e.g., ELITs of different size[9]). By using ultrafast high voltage switches to gate the end plates of the device (mirror-switching), ions can be selectively allowed to escape from the device through judicial timing of mirror-switching pulses. High-resolution ion isolations using mirror-switching, achieving an isolation resolution of > 35,000 (FWHM) for lipid isobars have been previously demonstrated.[10,11] This makes the ELIT a promising platform for tandem-MS, especially for complex mixtures containing isobaric species. While the isolation and high-resolution readout capabilities of the ELIT have been established, dissociation methods are needed to enable the ELIT to be operated as a stand-alone tandem mass spectrometer. Surface-induced dissociation (SID) of relatively small (<350 Da) singly-charged ions[12] and large multiply-charged protein complexes[13] has previously been demonstrated within an ELIT by placing a modified gold surface at one of the end plates. At each reflection at the endplates of the device, ions turn around ('turnaround point'), briefly having near zero kinetic energy. If fragmentation occurs at a turnaround point, minimal energy partitioning will occur between fragment ions, meaning

frequency to *m/z* calibration will not be further complicated. This allows for photofragmentation by simply focusing a laser through a turnaround point within the ELIT.

Photodissociation techniques such as infra-red multi-photon dissociation (IRMPD) and ultra-violet photodissociation (UVPD) have various applications in mass spectrometry. These include uses for increased sequence coverage in proteomics[14], generation of more informative fragments,[15] and for uses requiring a fragmentation process decoupled to ion trapping dynamics.[16] Photofragmentation is typically performed in linear quadrupole ion traps due to the stable storage of ions for long time periods, and radial confinement from collisional cooling. This allows for extended spatial overlap of ions with the laser beam. Photofragmentation has been performed in other mass analyzers, including FTICRs,[17] at the turnaround point for reflectrons in TOF,[18] and in ELITs.[19,20,21,22,23,24] In ELIT photodissociation, the laser beams were directed axially through the ELIT. For tandem-MS, this may present issues as fragmentation that occurs outside of the turnaround point will result in energy partitioning and ambiguous *m/z* assignments. To the best of our knowledge, this work is the first report of photodissociation exclusively at a turning point in an ELIT operating in conventional mass analysis mode. In this case, ions oscillating in the ELIT are exposed to a continuous beam of infra-red radiation directed orthogonally to the ion motion axis at a turning point to give rise to continuous-wave IRMPD (cw-IRMPD). In this setup, the ELIT itself is used as the mass analyzer for MS^2 spectra in FT mode, after mirror-switching isolation. The development of ion activation techniques in the ELIT is a key step towards its use in tandem MS, which would benefit from its high-resolution ion isolation capabilities.

2. Methods

2.1 Instrumentation

All experiments were performed on a home built ELIT instrument (**Figure 1**). Ions are generated using nano-electrospray ionization (nESI), passing through an interface region of approximately 900 mTorr. Ions pass through a conductance limiting aperture into the main chamber of the instrument at about $1x10^{-5}$ Torr. Ions are transmitted through a linear quadrupole ion guide and turned by a turning quadrupole into a linear quadrupole ion trap (LIT). After ions are formed and transferred into this LIT, the DC offset of this LIT is ramped from ~0 V to 1990 V. During this time, triangular electrodes inserted between the rods of this quadrupole (LINAC[25] electrodes) are ramped from ~0 V to 700 V. The potential difference between the rods and LINAC serves to bunch ions towards the exit lens of the LIT. Just prior to a gate-down of the exit lens to 1500 V and subsequent ion injection into the ELIT, ions are further bunched by lowering the exit lens voltage from 2000 V to 1980 V. Ions pass through a differentially pumped region between two conductance limiting apertures, guided by an Einzel lens, finally passing into the ELIT chamber held at ~$3x10^{-9}$ Torr. Ions enter the ELIT as the entrance plate is held at ~1600 V, after which this plate is gated up to the trapping voltage of ~2300 V. The delay between ion injection and the gate-up of this entrance plate determines the mass range of the instrument, as some spatial separation occurs in the region between the injection LIT and the ELIT. All voltage gates are performed using solid-state high voltage switches (HTS 31-03-GSM, Behlke Electronics GMBH, Kronberg,

Germany), with TTL pulses and timings controlled using a pulse/delay generator (model 575, Berkeley Nucleonics, San Rafael, CA).

2.2 cw-IRMPD

Two BaF_2 viewports were mounted to the ELIT chamber and positioned to allow transmission of the laser beam directly through the posterior turning point (i.e., between plates 7 and 8, see **Figure 1**) of the ELIT. A 40 Watt Synrad Firestar v40 laser (10.6 μm) was used for IRMPD. The beam was focused using a ZnSe lens with 149 mm focal length. Tuning of the beam position was accomplished via horizontal and vertical translation stages. The laser was continuous and was on for the duration of the irradiation phase of the experiment. A mirror switching pulse was used to remove ions from a portion of the fragment ion beam formed by the IRMPD to allow for FT analysis.

2.3 nESI

100 μM solutions of pYGGFL, pSGGFL, and KGAILPGAILR were prepared in 49:49:2 (by volume) solutions of water, methanol, and acetic acid. Ions were sprayed out of pulled borosilicate glass capillaries (50-100 μm diameter) for nano-electrospray ionization in positive ion-mode (1.2-1.5 kV) using the wire-in-a-capillary approach[26] to making electrical contact with solution.

2.4 Quantum computations

Quantum calculations of phospho-serine were performed using the QCHEM electronic structure package, version 2.15.3[27] The initial molecular structure was imported and optimized under 6-31G(d,p) basis set using DFT(B3LYP) in QCHEM. Following the optimized molecular structure, vibrational analysis including reduced masses, infrared activities and intensities was performed. All calculations were performed for gas-phase species, neglecting perturbations from intermolecular couplings potentially arising within the crystalline lattice.

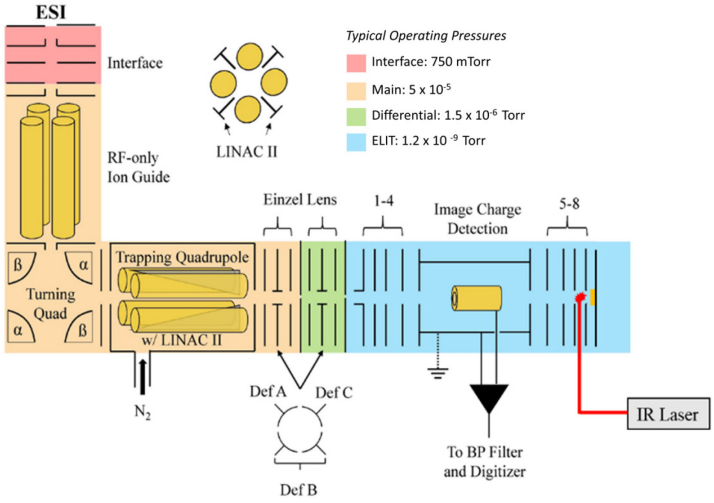

Figure 1: A schematic of the ELIT instrument with an IR laser path directed through the posterior turnaround point . A gold SID surface at the exit lens is also pictured, but not used here.

3. Results and Discussion:

3.1 Beam alignment

Precursor ion signal was used to tune for beam overlap with the ion packet. Transient lengths were approximately 300 ms after tuning of the ELIT plates, and pumping down to $3x10^{-9}$ Torr. Using a Hanning window for apodization of FT signal, depletion of precursor signal was readily observed upon alignment of the beam at 4 W laser power. The laser power was decreased while rastering the beam position until the optimal position for depletion was found. Despite significantly faster precursor depletion relative to the normal decay of transient signal from collisions with background gas, no fragment signal was initially observed. **Figure 2** shows a comparison of short-time Fourier transform (STFT) for a pYGGFL transient with no IR heating, and with the laser on.

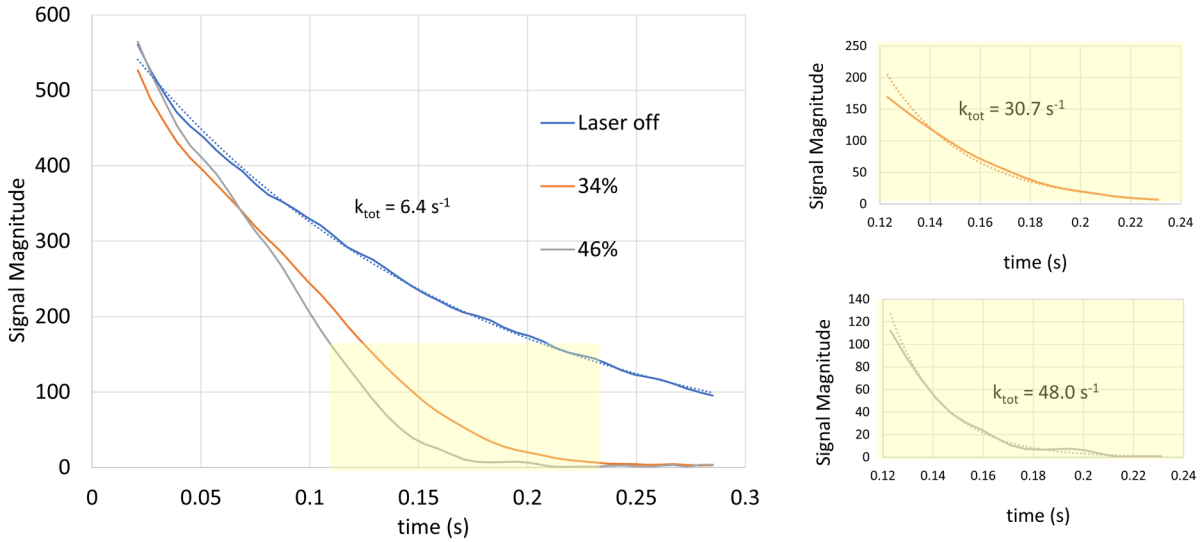

Figure 2: Extracted short-time Fourier transforms of three different $[pYGGFL+H]^+$ transients. STFTs were performed using 30 ms time-domain windows, and 6 ms step time. The blue trace shows the STFT of the precursor signal with no laser. The blue dotted line shows an exponential fit to the data. The orange and grey lines show STFTs of precursor signal with 34% and 46% laser power, respectively. The two insets on the right show zoomed in portions of the yellow highlighted region in the main plot, for the 34%, and 46% laser power STFTs. These are fitted with exponential fits shown by the dotted lines.

3.2 Laser power absorption in the ELIT

Because negligible collisional cooling occurs in high vacuum ($3x10^{-9}$ Torr) in the ELIT, ions under IR irradiation will reach a steady state internal temperature distribution approximately governed

by the Planck relation.[28] After the laser is turned on, time is required to heat the ion population to a temperature distribution that overlaps with the fragmentation energy threshold. **Figure 2** shows the STFTs of precursor signal for pYGGFL at 0%, 34%, and 46% laser power. At each of the three laser powers shown, the decay rate at the early portion of the transient is similar, and thus results primarily from collisions with neutral background gas. At around 60 ms, the STFT for 34% and 46% laser power show an increased decay rate, as the temperature distribution of precursor ions begins to overlap with the fragmentation threshold. The insets in **Figure 2** show exponential fits to the later sections of the STFTs of precursor intensity for 34% and 46% laser power. If a steady state internal temperature distribution were reached, a constant dissociation rate due to IR activation would be expected.[23]

While the blackbody infrared radiative dissociation (BIRD) method[29,30] for the study of gas phase thermal unimolecular dissociation kinetics can, in principle, extend to experiments using IR lasers as a radiation source, it is difficult to obtain the effective temperature of ions under laser irradiation, making interpretation of results difficult. In the case of a laser directed orthogonally to the ELIT axis, the ability to study dissociation energetics is further complicated by the dynamic ion overlap with the incident laser. To better understand the dynamics of the ELIT experiment, the absorption cross section of phospho-serine was calculated using the Q-Chem 6.0 software to be 8.9×10^{-20} cm^2. Using the relation $k_{diss} = P(E_t - hv, E_t)\sigma I$, where $P(E_t - hv, E_t)$ is the probability a given molecule will exist between a fragmentation energy threshold E_t and one photon energy lower, σ is the absorption cross section, and I is the laser intensity,[27] the expected rate constant at a given laser intensity can be calculated. Here, the energy threshold E_t is the energy at which dissociation becomes faster than the up-pumping rate from absorption. An upper limit to the photodissociation rate can be obtained by assuming by assuming all ions are one photon away from the energy threshold (i.e., $P(E_t - hv, E_t) = 1$). With this assumption, the expected dissociation rate for a laser power of 10 Watt is 8,840 s^{-1}. The time an ion spends in the focused laser beam waist during each lap (assuming the focal point is at the turnaround point), is roughly 2.5% of the total oscillation time (assuming a linear potential gradient at the turning point and no radial component in ion trajectory). Thus, the maximum expected decay rate in the ELIT would be 8,840 s^{-1} x 2.5% = 226 s^{-1}. The estimated dissociation rates in **Figure 2** are substantial fractions of the maximum, which suggests a large value of $P(E_t - hv, E_t)$, or a large fraction of ions dissociating at the laser up-pumping rate or faster.[27] The Boltzmann temperature distribution for such high dissociation rates may therefore be heavily truncated or not at equilibrium.[27] This suggests that so-called 'rapid energy exchange' conditions are not achieved under these conditions such that extensive modelling would be required to derive reliable activation parameters from measurement of the dissociation rates.

3.3 Recovery of FT signal

The lack of FT signal for fragment ions after the observed depletion, as well as the constant rate of decay owing to fragmentation during the experiment indicate that fragments are formed each lap after the initial heating occurs. Due to the lap time difference between the precursor and

fragment ions, fragments are not generated at identical phase relative to one another. After prolonged fragment formation, the result is a homogenous fragment ion beam (i.e., the ions are not moving coherently). Specifically, the measured lap time of the $[pYGGFL + H]^+$ precursor ion in figure 2 is ~13.4 µs, while the oscillation beat period between this ion and its corresponding water loss peak is about 930 µs. In contrast, irradiation times required for sufficient fragmentation were >50 ms, meaning the entire range of possible phase differences between the precursor population and fragments formed would be explored in these experiments. To recover FT signal from the consequent ion beam of fragments, a mirror-switching isolation pulse was applied after the irradiation period to remove a portion of the ion beam (see schematic diagram at the top of **Figure 3**). This introduces some variation on the charge detected from the ion beam by the pickup detection electronics. The gap in the fragment ion beam oscillates at the characteristic frequency of the fragment ions. **Figure 3** shows mass spectra of pYGGFL after irradiation both with and without a mirror-switching pulse. The presence of an additional water loss peak in the spectrum with the mirror-switching pulse indicates that a fragment beam was present, and perturbed as described. The width of this mirror-switching pulse was empirically optimized to be 1 µs, while the delay (phase) of the pulse had no effect on fragment signal, indicating a homogenous beam. The difference in isotope intensities between the two spectra for the precursor ion population in **Figure 3**, which moves coherently, is due to the mirror-switching pulse used to recover fragment ion signal, which also caused ejection of these ion packets from the ELIT.

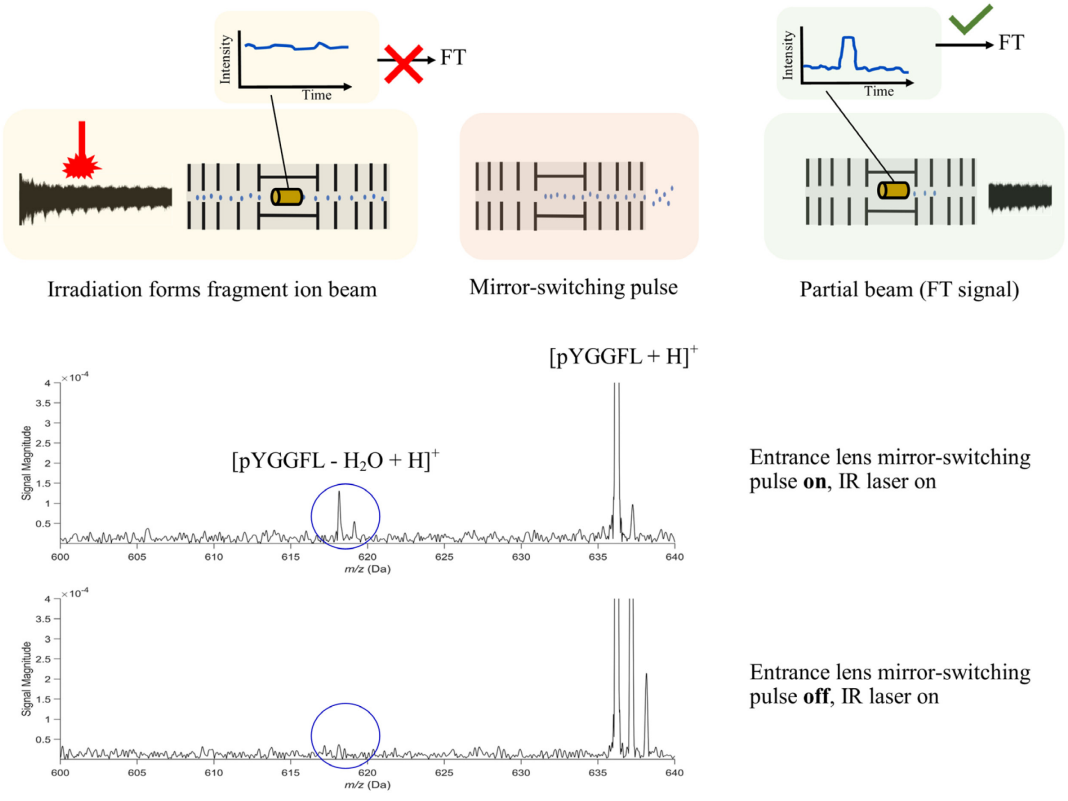

Figure 3: Top: Diagram of the experimental sequence. Ions are irradiated for 100 ms, followed by a mirror switching pulse of 1 μs width to perturb part of the fragment ion beam prior to FT readout. Bottom: comparison of spectra with and without the mirror-switching FT signal recovery pulse.

3.4 Potential energy partitioning effects

The mirror-switching FT signal recovery method described above has been shown to be effective at revealing product ions from every precursor ion studied to date. For example, a y_6^{2+} fragment peak was observed when $[KGAILPGAILR+3H]^{3+}$ was irradiated, and a water loss, b_4, and a_4 fragments were observed upon irradiation of $[pYGGFL+H]^+$. The richest fragmentation spectrum was observed with pSGGFL, where water loss, phosphoric acid loss, and a_4 and b_4 fragments were observed. However, a commonality among these spectra is that the fragments observed were all close in *m/z* to the precursor, with the furthest in *m/z* being the a_4 fragment at ~159 *m/z* units from the precursor *m/z*. **Figure 4**, for example, shows the MS^2 spectrum of $[pSGGFL+H]^+$, where all observed fragments are close in *m/z* to the precursor. This phenomenon might arise from fragmentation that does not occur precisely at the turning point. When fragmentation occurs, a fragment ion will retain a portion of the precursor kinetic energy proportional to its mass fraction. Because the ELIT is well-tuned for stable confinement of ions of a narrow kinetic energy to charge ratio range, only ions with minimal kinetic energy partitioning will be efficiently stored following fragmentation. The apparent discrimination in favor of fragments of similar *m/z* to that of the precursor suggests that fragmentation is occurring while the kinetic energy of ions is not exactly zero. Tuning based on the maximal loss of precursor ion was done assuming that this would occur at the turning point. However, these results might indicate that the site with greatest precursor ion overlap with the laser may not occur at the turning point.

Figure 4: Overlayed spectra of pSGGFL both with (black) and without (blue) IR irradiation for 100 ms of the transient. A 1 μs mirror-switching pulse is used to recover FT signal after the irradiation period.

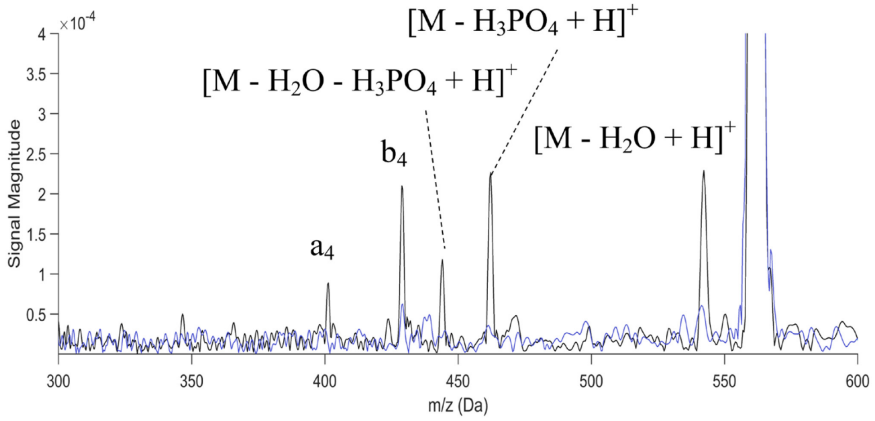

4. Summary and Conclusions

Cw-IRMPD at rates of 30-50 s^{-1} is demonstrated at the turnaround point of an ELIT. At such rates, rapid energy exchange conditions are not expected. The slow heating nature of IRMPD gives rise to fragments being generated over relatively long periods of time, thereby resulting in a lack of coherence of product ions due to the lap time difference between precursor and product ions. This scenario precludes fragment ion detection via image current measurement. In order to generate a product ion spectrum, a mirror-switching event can be used to introduce a notch in the otherwise homogeneous product ion beam that oscillates at the frequency of the product ion. The combination of IRMPD fragmentation and mirror-switching isolation allows for tandem MS to be performed within the ELIT mass analyzer. However, the results described herein suggest that there may be discrimination against low *m/z* product ions, which can result when fragmentation takes place away from the turning point. An alternative to introducing a notch in the product ion beam to address the issue associated with the generation of a homogeneous fragment ion beam would be to transfer the product ions into a quadrupole linear ion trap for re-bunching. The issue with low *m/z* discrimination, on the other hand, will require a more precise location of the dissociation event at the turning point. Some improvement might be obtained via an alternative approach to adjusting the location of the laser, which was optimized simply by maximizing ion depletion in this work. In any case, it is desirable to effect more prompt dissociation, which calls for a faster form of activation, such as surface-induced dissociation or ultraviolet photodissociation.

ACKNOWEDLMENTS

The authors acknowledge support from the National Science Foundation NSF CHE-1708338 and Sciex for providing the quadrupole linear ion trap with LINAC electrodes and for supporting the construction of the original version of the ELIT system.

DATA AVAILABILITY STATEMENT

The data that support the findings in this work are available from the corresponding author upon reasonable request.

AUTHOR CONTRIBUTION INDICATION

Ian J. Carrick: Conceptualization, methodology, investigation, visualization, writing

Kimberly C. Fabijanczuk: Conceptualization, methodology, investigation, visualization

Jiayue Rong: Conceptualization, methodology, visualization

Scott A. McLuckey: Conceptualization, writing – review and editing, supervision, project administration

ORCID

Scott A. McLuckey https://orcid.org/0000-0002-1648-5570

References

1 Zajfman D, Heber O, Vejby-Christensen L, Ben-Itzhak I, Rappaport M, Fishman R, Dahan M. Electrostatic bottle for long-time storage of fast ion beams. *Phys Rev A*. 1997;55(3):R1577-R1580. doi:10.1103/PhysRevA.55.R1577

2 Dziekonski, E. T., Santini, R. E., & McLuckey, S. A. (2016). A dual detector Fourier transform electrostatic linear ion trap utilizing in-trap potential lift. *International Journal of Mass Spectrometry*, *405*, 1–8. doi: 10.1016/j.ijms.2016.05.010

3 Pedersen HB, Strasser D, Heber O, Rappaport ML, Zajfman D. Stability and loss in an ion-trap resonator. *Phys Rev A*. 2002;65(4):042703. doi:10.1103/PhysRevA.65.042703

4 Dziekonski ET, Johnson JT, Lee KW, McLuckey SA. Fourier-Transform MS and Closed-Path Multireflection Time-of-Flight MS Using an Electrostatic Linear Ion Trap. *Anal Chem*. 2017;89(20):10965-10972. doi:10.1021/acs.analchem.7b02797

5 Zajfman D, Rudich Y, Sagi I, Strasser D, Savin D.W, Goldberg S, Rappaport M, Heber O. High resolution mass spectrometry using a linear electrostatic ion beam trap. *International Journal of Mass Spectrometry*. 2003;229(1-2):55-60. doi:10.1016/S1387-3806(03)00255-0

6 Strasser D, Geyer T, Pedersen HB, Heber O, Goldberg S, Amarant B, Diner A, Rudich Y, Sagi I, Rappaport M, Tannor D.J, Zajfman D. Negative Mass Instability for Interacting Particles in a 1D Box: Theory and Application. *Phys Rev Lett*. 2002;89(28):283204. doi:10.1103/PhysRevLett.89.283204

7 Shockley W. Currents to Conductors Induced by a Moving Point Charge. *Journal of Applied Physics*. 1938;9(10):635-636. doi:10.1063/1.1710367

8 Zubarev RA, Makarov A. Orbitrap Mass Spectrometry. *Anal Chem*. 2013;85(11):5288-5296. doi:10.1021/ac4001223

9 Johnson JT, Lee KW, Bhanot JS, McLuckey, SA. A Miniaturized Fourier Transform Electrostatic Linear Ion Trap Mass Spectrometer: Mass Range and Resolution. *J. Am. Soc. Mass Spectrom.* 2019;30:588-594. doi:10.1007/s13361-018-02126-x

10 Johnson JT, Carrick IJ, Eakins GS, McLuckey SA. Mirror Switching for High-Resolution Ion Isolation in an Electrostatic Linear Ion Trap. *Anal Chem*. 2019;91(14):8789-8794. doi:10.1021/acs.analchem.9b00874

11 Johnson JT, Carrick IJ, Eakins GS, McLuckey SA. Simultaneous Isolation of Nonadjacent *m*/*z* Ions Using Mirror Switching in an Electrostatic Linear Ion Trap. *Anal Chem*. 2019;91(19):12574-12580. doi:10.1021/acs.analchem.9b03560

12 Hilger RT, Santini RE, McLuckey SA. Nondestructive Tandem Mass Spectrometry Using a Linear Quadrupole Ion Trap Coupled to a Linear Electrostatic Ion Trap. *Anal Chem*. 2013;85(10):5226-5232. doi:10.1021/ac4007182

13 Carrick IJ, Johnson JT, McLuckey, SA. Surface-induced Dissociation of Protein Complex Ions in a Modified Electrostatic Linear Ion Trap. *Int. J. Mass Spectrom.* 2023; 496: 1117170. doi.org/10.1016/j.ijms.2023.117170

14 Greisch JF, van der Laarse SAM, Heck AJR. Enhancing Top-Down Analysis Using Chromophore-Assisted Infrared Multiphoton Dissociation from (Phospho)peptides to Protein Assemblies. *Anal Chem*. 2020;92(23):15506-15516. doi:10.1021/acs.analchem.0c03412

15 Robinson MR, Taliaferro JM, Dalby KN, Brodbelt JS. 193 nm Ultraviolet Photodissociation Mass Spectrometry for Phosphopeptide Characterization in the Positive and Negative Ion Modes. *J Proteome Res*. 2016;15(8):2739-2748. doi:10.1021/acs.jproteome.6b00289

16 Theisen A, Wootton CA, Haris A, Morgan T.E, Lam Y.P.Y, Barrow, M.P, O'Connor, P.B. Enhancing Biomolecule Analysis and 2DMS Experiments by Implementation of (Activated Ion) 193 nm UVPD on a FT-ICR Mass Spectrometer. *Anal Chem*. 2022;94(45):15631-15638. doi:10.1021/acs.analchem.2c02354

17 Bowers WD, Delbert SS, Hunter RL, McIver RT. Fragmentation of oligopeptide ions using ultraviolet laser radiation and Fourier transform mass spectrometry. *J Am Chem Soc*. 1984;106(23):7288-7289. doi:10.1021/ja00335a094

18 Cornett DS, Peschke M, LaiHing K, Cheng PY, Willey KF, Duncan MA. Reflectron time-of-flight mass spectrometer for laser photodissociation. *Review of Scientific Instruments*. 1992;63(4):2177-2186. doi:10.1063/1.1143135

19 Johnson CJ, Shen BB, Poad BLJ, Continetti RE. Photoelectron-photofragment coincidence spectroscopy in a cryogenically cooled linear electrostatic ion beam trap. *Review of Scientific Instruments*. 2011;82(10):105105. doi:10.1063/1.3641875

20 Halim MA, Clavier C, Dagany X, Keleroux M, Dugourd P, Dunbar R.C, Antoine, R. Infrared laser dissociation of single megadalton polymer ions in a gated electrostatic ion

trap: the added value of statistical analysis of individual events. *Phys Chem Chem Phys*. 2018;20(17):11959-11966. doi:10.1039/C8CP00404H

21 Fischer P, Schweikhard L. Photofragmentation of Bin+/- clusters (n = 2−19) in an electrostatic ion beam trap. *Eur Phys J D*. 2019;73(5):105. doi:10.1140/epjd/e2019-100027-0

22 Doussineau T, Paletto P, Dugourd P, Antoine R. Multiphoton Dissociation of Electrosprayed MegaDalton-Sized DNA Ions in a Charge-Detection Mass Spectrometer. *J Am Soc Mass Spectrom*. 2015;26(1):7-13. doi:10.1007/s13361-014-1011-z

23 Doussineau T, Antoine R, Santacreu M, Dugourd P. Pushing the Limit of Infrared Multiphoton Dissociation to Megadalton-Size DNA Ions. *J Phys Chem Lett*. 2012;3(16):2141-2145. doi:10.1021/jz300844e

24 Antoine R, Doussineau T, Dugourd P, Calvo F. Multiphoton dissociation of macromolecular ions at the single-molecule level. *Phys Rev A*. 2013;87(1):013435. doi:10.1103/PhysRevA.87.013435

25 Loboda A, Krutchinsky A, Loboda O, McNabb J, Spicer V, Ens W, Standing K. Novel LINAC II electrode geometry for creating an axial field in a multipole ion guide. *Eur J Mass Spectrom.* 2000;6,531-536.

26 Van Berkel GJ, Asano KG, Schnier PD. Electrochemical processes in a wire-in-a-capillary bulk-loaded nano-electrospray emitter. *J Am Soc Mass Spectrom* 2001;12:853-862.

27 Shao Y, Gan Z, Epifanovsky E, Gilbert ATB, Wormit M, Kussmann J, Lange AW, Behn A, Deng J, Feng X, Ghosh D, Goldey M, Horn PR, Jacobson LD, Kaliman I, Khaliullin RZ, Kuś T, Landau A, Liu J, Proynov EI, Rhee YM, Richard RM, Rhordanz,MA, Steele RP, Sundstrom EJ, Woodcock III HL, Zimmerman PM, Zuev D, Albrecht B, Alquire E, Austin B, Beran GJO, Bernard YA, Berquist E, Brandhorst K, Bravaya KB, Brown ST, Casanova D, Chang C-M, Chen Y, Chien SH, Closser, KD, Crittenden DL, Diedenhofen M, Distasio Jr. RA, Do H, Dutoi AD, Edgar RG, Fatehi S, Fusti-Molnar L, Ghysels An, Golubeva-Zadorozhnaya A, Gomes J, Hanson-Heine MWD, Harbach PHP, Hauser AW, Hohenstein EG, Holden ZC, Jagau T-C, Ji H, Kaduk B, Khistyaev K, Kim J, Kim, J, King RA, Klunzinger P, Kosenkov D, Kowalczyk T, Krauter CM, Lao KU, Laurent AD, Lawler KV, Levchenko SV, Lin CY, Liu F, Livshits E, Lochan RC, Luesner A, Manohar P, Manzer SF, Mao S-P, Mardirossian n, Marenich AV, Maurer SA, Mayhall NJ, Neuscamman E, Oana CM, Olivares-Amaya R, O'Neill DP, Parkhill JA, Perrine TM, Peverati R, Prociuk A, Rehn DR, Rosta E, Russ NJ, Sharada SM, Sharma S, Small, DW,

Sodt, A, Stein T, Stück D, Su Y-C, Thom AJW, Tsuchimochi T, Vanovschi V, Vogt L, Vydrov O, Wang T, Watson MA, Wenzel J, White A, Williams CF, Yang J, Yeganeh S, Yost SR, You Z-Q, Zhang IY, Zhang X, Zhao Y, Brooks BR, Chan GKL, ChipmanDM, Cramer CJ, Goddard III WA, Gordon MS, Hehre WJ, Klamt A, Schaefer III HF, Schmidt MW, Sherrill CD, Dunietz BD, Furlani TR, Gwaltney SR, Hsu C-P, Jung Y, Kong J, Lambrecht DS, LianWZ, Ochsenfeld C, Rassolov VA, Slipchenko LV, Subotnik, JE, Voorhis TV, Herbert JM, Krylov AI, Gill PMW, Head-Gordon M. Advances in molecular quantum chemistry contained in the Q-Chem 4 program package. *Molecular Physics*, 2015;113(2), 184–215. https://doi.org/10.1080/00268976.2014.952696

28 Dunbar RC. Kinetics of low-intensity infrared laser photodissociation. The thermal model and application of the Tolman theorem. *J Chem Phys.* 1991;95(4), 2537–2548. doi: 10.1063/1.460958

29 Schnier PC, Price WD, Jockusch RA, Williams ER. Blackbody infrared dissociation of bradykinin and its analogues: Energetics, dynamics, and evidence for salt-bridge structures in the gas phase. *J. Am. Chem. Soc.* 1996;118(30),7178-7189. doi.org/10.1021/ja9609157

30 Dunbar RC. BIRD (Blackbody Infrared Radiative Dissociation): Evolution, Principles, and Applications. *Mass Spectrom. Rev.* 2004;23,127-158.